ABSTRACT

DONG, JU. Mechanical Property Enhancement by Post-fabrication of Thermal Curing of Core-sheath Epoxy Fibers. (Under the direction of Dr. Russell Gorga and Dr. Laura Clarke).

A Strategy is described to prepare epoxy-polymethyl methacrylate (PMMA) core-sheath fiber via co-axial electrospinning. The core solution is composed of pre-cured epoxy, hardener, gold nanoparticles (AuNPs), perylene and dimethylformamide (DMF). Perylene is used for monitoring temperature changes during photothermal curing. DMF is used to adjust the viscosity of the core solution which makes the co-axial electrospinning more controllable. Since the AuNPs are easily attacked by the hardener, epoxy – hardener is partially cured (for 10 hours at room temperature) before mixing with the AuNPs. Followed by bath sonication, AuNPs are well dispersed into the core solution. Core-sheath epoxy fibers are cured in an oven after fabrication. Thermogravimetric analysis shows that core-sheath epoxy fibers are fully cured after 2 hours at $60^{o}C$. Unique fiber morphologies (including U-shape, fiber bundle and ribbon-like) are observed under scanning electron microscopy and transmission electron microscopy after curing, which is mainly due to the exothermal heat generated during epoxy curing reaction. After selective removal of the PMMA sheath by washing, fiber average diameter decrease from 1.32 µm to 0.79 µm. Fourier transform infrared spectroscopy shows that the core-sheath epoxy fibers after washing display diminished PMMA signal and more pronounced epoxy signal, which indicates that majority of PMMA is removed after washing. Mechanical properties are compared between pure PMMA fibers, core-sheath epoxy fibers and fibers after washing. Dynamitic mechanical analysis shows that core-sheath epoxy fibers has better mechanical performance (with the best performance after 3 hours

curing) than pure PMMA fibers, and core-sheath epoxy fibers show similar performance to epoxy core-sheath fibers.

Mechanical Property Enhancement by Post-fabrication of Thermal Curing of Epoxy Core-sheath Fibers

by
Ju Dong

A thesis submitted to the Graduate Faculty of
North Carolina State University
in partial fulfillment of the
requirements for the degree of
Master of Science

Textile Chemistry

Raleigh, North Carolina

2014

APPROVED BY:

Dr. Russell Gorga Committee Co-Chair	Dr. Laura Clarke Committee Co-Chair
Dr. Wendy Krause	Dr. Kevin Gross

DEDICATION

This work is dedicated to my family and friends.

BIOGRAPHY

Ju Dong was born in 1990 in the city of Zibo, Shandong Province. Influenced by his parents, he chose light-chemical engineering as his major at Jiangnan University in 2008. He started working on electrospinning and phase change materials since his junior year at Jiangnan University. He came to the College of Textiles at North Carolina State University in 2012 and started working with Dr. Russell Gorga in spring 2013 and with Dr. Laura Clarke in fall 2013. Out of lab, he enjoys listening to metal. His favorite band is Insomnium.

ACKNOWLEDGMENTS

I would like to thank the TECS department and Dr. Gorga for their support. I would also like to thank Dr. Gorga and Dr. Clarke and Dr. Bochinski for their guidance on this work. In addition, I would like to thank Dr. Krause and Dr. Gross for serving as my committee member. Many thanks are due to my lab-mates - Mr. Gabriel Firestone and Mr. Colin Curtis for their helpful discussion.

I acknowledge the AIF staff, Ms. Judy Elson, Ms. Birgit Anderson and Mr. Jialong Shen for their equipment help.

Last but definitely not the least, I do appreciate my family and friends for their support and continuous love.

TABLE OF CONTENTS

LIST OF TABLES

LIST OF FIGURES

CHAPTER 1

Introduction and Background

1.1 Historical Overview of Traditional One-nozzle Electrospinning

Today, electrospinning has proved to be an effective method of fabricating fibers at the micro/nano scale. In late 16^{th} century, English physician - William Gilbert [1] pointed out that a droplet of water would form a cone shape and would be ejected from the tip of the cone under electric field. This is believed to be the first description of electrospinning phenomenon. In 1900, American scientist John F, Colley [2] declared the invention of a new and useful apparatus for electrically dispelling fluids, which was the first patent related to electrospinning. Between 1964 and 1969, Geoffrey Taylor [3-5] published three papers in which he mathematically modeled the shape of the cone formed by the droplet fluid under the electric field. Hence, the cone was named after him as the Taylor cone. Since 1995, Darrel Reneker [15] published a series of paper developing electrospinning mechanics in both theoretical and experimental ways. Jumping into 21 century, scientists began realizing the application of electrospun fibers in many areas due to their high porosity and large surface area to volume ratio. Since then, the number of publications related to electrospinning has been increasing exponentially every year [6].

1.2 Overview of Co-axial Electrospinning

Most recently, core-sheath configuration started to gain interest due to its further enhanced material property profile over one layer structure. Core-sheath fibers provides possibility for achieving unique profiles that are difficult to obtain by fabricating two consistent materials separately and adhered together subsequently.

Before the invention of co-axial electrospinning, methods of fabrication of core-sheath fibers included laser ablation [7], polymerization of monomers on a template [8], and growing a semiconductor nanowire inside the polymer tubules [9]. Micro/nano scale polymer-metals and polymer-polymer fibers were also obtained by the tubes by fiber templates (TUFT)-process [10-11]. In 2003, an Israel research group [12] developed a new technology based upon traditional one-nozzle electrospinning which is called co-axial electrospinning. Figure 1.1 depicted co-axial electrospinning set-up. Both liquid outflowing from the core and the sheath were polymer solutions (recent research indicated that core solution could be non-polymeric solution, such as mineral oil). A compound droplet sustained at the tip of compound nozzles and thereby should undergo transformation into a compound Taylor cone and ejected a compound jet. Co-axial electrospinning working process is similar to that of traditional one-nozzle electrospinning. The compound jet would be pulled under the electric field and stretched before it went into elongation and whipping section. The compound jet broke into multiple jets in whipping section, and solvent would evaporate fast before attaching collector and form solid fibers. However, to form core-sheath structure instead of random blended structure, the co-axial electrospinning should be expected to be fast enough to prevent any mixing of the core and sheath in the compound Taylor cone/or jet.

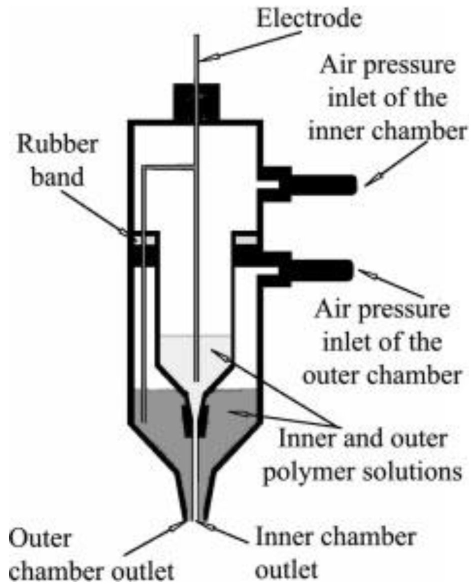

Figure 1.1 Experimental set-ups for co-axial electrospinning

1.3 Driving Parameters in Co-axial Electrospinning

Similar to traditional one-nozzle electrospinning, co-axial electrospinning is determined by parameters such as material itself (including miscibility or immiscibility of the pair of solutions, viscosity, and surface tension), applied voltage, and sheath-to-core flow rate ratio. Such parameters will be discussed separately in the following paragraphs.

1.3.1 Materials

1.3.1.1 Solution Viscosity

In co-axial electrospinning, the viscosity of the sheath solution is required to be such that the Maxwell stress imparted by it on the core is sufficient to overcome the surface tension between the two solutions, and therefore allows the formation of a compound Taylor cone and jet [12]. According to our experience, viscosity of the sheath solution is critical in the formation of core-sheath Taylor cone in co-axial electrospinning. Most importantly, the sheath polymer should be electrospinnable by itself which means the sheath should be viscous enough to possess enough entanglements [13]. Based on Yarin's paper in 2006 [14], it seemed that a well-stabilized co-axial electrospinning process could be achieved when both solutions were sufficiently viscous. In addition, co-axial electrospinning was easier to be accomplished when the solutions were immiscible. Yu [13] shared similar idea with Yarin. He also suggested that although the core and sheath solutions could be miscible, co-axial electrospinning was less controllable since mutual diffusion could take place in the core-sheath Taylor cone and jet. He also brought up two hypotheses explaining why the jet break-up of the core fluid could be prevented by the sheath via two mechanisms: 1) strain hardening of the interface between the sheath and the core due to rapid stretching that occurred during whipping section; 2) lesser surface forces acting on the core solution surrounded by the sheath, which otherwise would be higher if the contact of the core was with air, also would be true if the core material was electrospinnable by itself. However, several studies [12, 16-17] still observed jet break-up of the core when the viscosity of the core was too low. Accordingly, the core solution must possess a certain minimum viscosity if it would like to be entrained continuously without break-up.

1.3.1.2 Solution Concentration

In traditional one-nozzle electrospinning, the increase in solution concentration will no doubt increase the fiber diameter due to more material flowing out in a fixed time, and verse versa.

Similarly, this effect of solution concentration also applied to co-axial electrospinning but will be more complicated. Zhang [18] conducted a series of experiments with the increase of core concentration while keeping sheath concentration constant. He showed that the increase in the core concentration increased both the core diameter and entire fiber diameter. In addition, they found that with the increase in the core diameter, the sheath size decreased, which was due to the same mass of the sheath distributed over a larger core. Similarly, He [17] observed an increase in the entire fiber diameter when he used higher sheath concentration and keeping the core concentration constant. This was due to the increase in the sheath size.

1.3.1.3 Solvent/Solution Miscibility and Immiscibility

Most importantly, the core and sheath solutions should not react with each other when they meet at the tip of the needle. Secondly, the interfacial tension between the core and the sheath should be as low as possible in order to form stable Taylor cone [13].

Li and Xia [20] reported that mixing between the core and sheath solutions could occur in the compound droplet at the tip of the needle if they were miscible or they were both dissolved in miscible solvent. In their papers, they used two immiscible solutions - PVP and the ceramic precursor $Ti(OiPr)_4$ dissolved in ethanol as the sheath, and mineral oil as the core, and obtained uniform hollow fibers after extraction of the oil out of the mineral oil/PVP-$Ti(OiPr)_4$ core-sheath electrospun fibers.

On the other hand, even though Yarin declared that miscible solutions were more controllable in co-axial electrospinning, researchers diverged on this statement. Sun [19] showed that “the characteristic time of diffusion spreading of a boundary” between two miscible solutions was greater than that of the electrospinning process and therefore no mixing took place. They supported this hypothesis by using PEO dissolving in a water-ethanol mixture for both the sheath and the core, only differing in the concentration, and successfully get PEO-PEO core-sheath fibers. Rutledge [13] was in agreement with this hypothesis and he stated that using the same solvent might also help reduce the interfacial tension between the core and sheath solutions, which should further lead to the formation of an uniform core-sheath fiber. In addition, other studies [13, 17, 21, 22] also reported the use of miscible or even same solvent for both the core and sheath, and successfully obtain core-sheath fibers.

1.3.1.4 Solution Conductivities

Solutions characterized by high conductivity have high surface charge density, which will lead to an increase in the elongation force on the jet due to self-repulsion of the excess charges under electric field. Hence, higher solution conductivity help produce smaller fibers in co-axial electrospinning [23, 24].

Conductivity difference between the sheath and the core solutions can also affect the formation of core-sheath fiber. Yu [13] speculated that higher sheath conductivity would not limit the formation of core-sheath fiber, but would increase shear stress to the core material and result in a thinner core. As discussed above, even the core solution is non-conductive, as long as the sheath solution is conductive and electrospinnable, core-sheath fibers can still be achieved with suitable parameters [20].

1.3.2 Applied Voltage

In co-axial electrospinning, applied voltage determines the electric field strength and further influence the formation of compound jet. One particular fact in co-axial electrospinning is that only the sheath solution is charged and ejected by electric force, whereas the core is stretched by Maxwell stress. Moghe [25] reported that for fixed parameters of the core and sheath polymer solutions, there existed a range of applied voltage within which a stable compound Taylor cone would form (Figure 1.2). This range varied with the type of polymers used. Voltage below the lower critical voltage (Figure 1.2 A) caused dripping. In addition, since the droplet at the tip of the needle became bigger, mixing of the two solutions tended to occur if the two solutions were miscible. Voltage above the upper critical voltage (Figure 1.2 C) caused the strength of the electric field to exceed that required for the polymers and the processing conditions and Taylor cones tended to recede and jets tended to inject from inside the capillaries. This resulted in multiple jets from the sheath solution (Figures 1.3) and no core-sheath fibers formed.

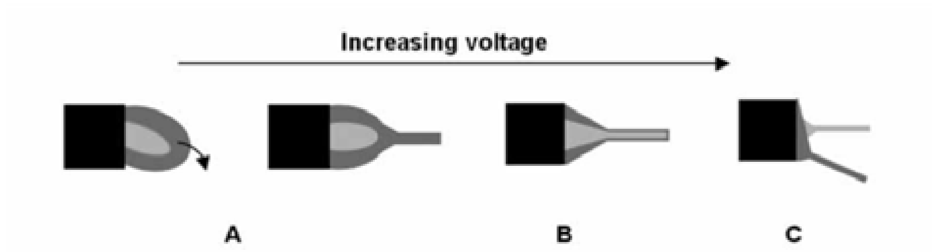

Figure 1.2 Schematic of the voltage dependence of the core-sheath fiber formation in co-axial electrospinning (A: Below critical voltage; B: At critical voltage; C: Above critical voltage)

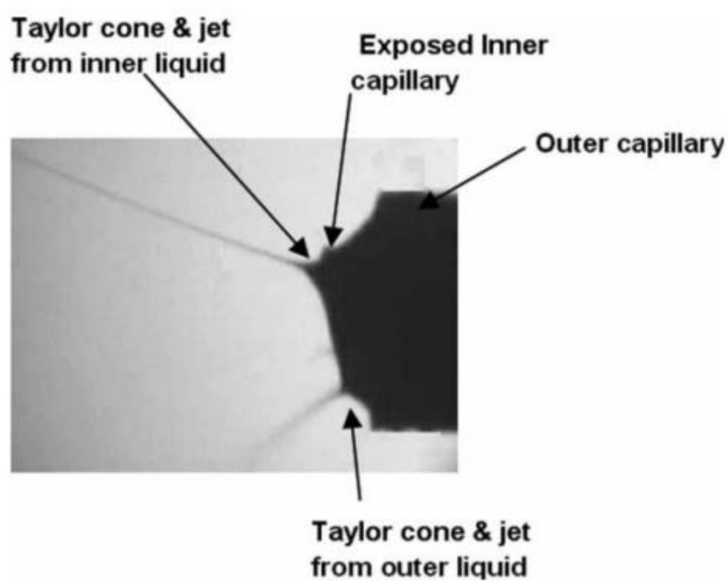

Figure 1.3 Separate fluid jets formed above critical voltage

In previous work, we also yielded similar results which will be shown in Appendix B.

1.3.3 Flow Rates of Core and Sheath Solutions

There is no doubt that the flow rates directly determine the size of the sheath and the core layers in co-axial electrospinning. In previous work, we observed that while fixing the sheath flow rate, there existed a range of core flow rates within which would form stable core-sheath Taylor cone and resulting in core-sheath fibers. That said, if the core flow rate is too low, the support of the core solution will be insufficient, and will occur discontinuous incorporation of the core into the sheath, and finally uneven core-sheath fibers. On the other hand, if the core flow rate is too high, the size of the core-sheath Taylor cone will increases beyond the point that the surface tension applied by the sheath solution is insufficient to confine the core solution within the cone. This will cause the inner cone to lose its characteristic shape and even result into the mixing of core and sheath solution or dripping of compound droplet [12]. In other words, the sheath fails to encapsulate the fast moving core uniformly and renders the overall process unstable [13, 26]. Hence, the core flow rate should generally be lower than that of the sheath in co-axial electrospinning.

1.4 Applications of Co-axial Electrospinning

With the combination of co-axial electrospinning and post-fabrication, fibers made up of non-electrospinnable materials, hollow fibers and fibers containing small particles could be achieved successfully. Below will be a few examples of each type of fibers.

1.4.1 Fibers Made Up of Non-electrospinnable Materials

With the help of co-axial electrospinning, the sheath would act as template and guide the non-electrospinnable core materials to form fibers. Usually, core fibers are obtained after removing the sheath by dissolving in suitable solvent (Figure 1.4). It is worth noting that the pre-requisite for this approach to make core fibers is that the sheath polymer is electrospinnable by itself.

Figure 1.4 Schematic of formation of fibers made up from non-electrospinnable material

Ojha [27] successfully fabricated chitosan nanofibers by dissolving chitosan-PEO core-sheath fibers in water. The chitosan fibers had a diameter around 100nm and appeared flatter and ribbon-like morphology due to swelling after washing (Figure 1.5). However, the obtained chitosan mat was extremely fragile because the dilute inner chitosan solution for process optimization failed to have sufficient chain entanglements to give satisfied mechanical properties. Therefore, no potential applications of such chitosan nanofibers were claimed.

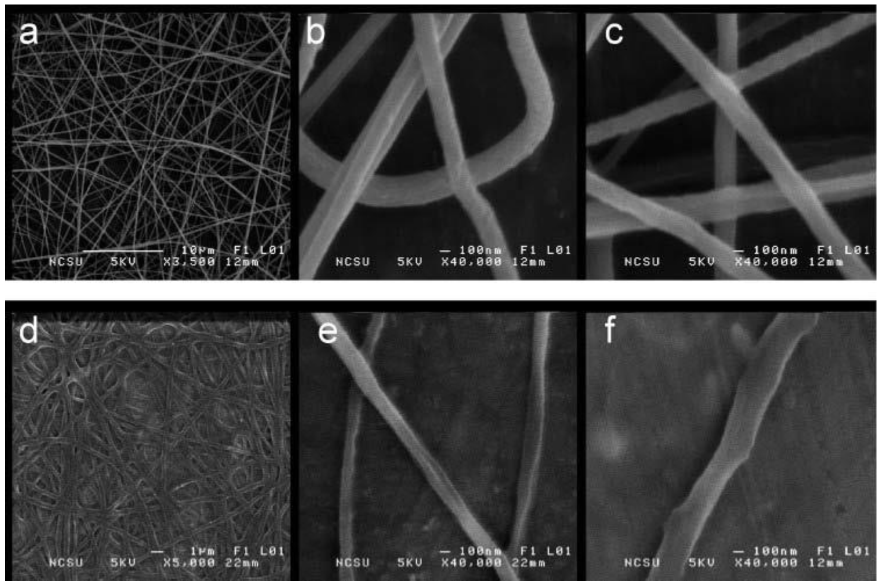

Figure 1.5 SEM images of electrospun chitosan-PEO core-sheath nanofibers. (a-c) samples before H_2O rinse and (d-f) samples after H_2O rinse

Yu [29] developed a modified coaxial electrospinning process using a pure solvent as sheath to assist the core solution in forming fiber. He pointed out that N,N-dimethylacetamide (DMAc) with lower vapor pressure prevented rapid loss of the core solvent, averting gel-like skin or clogging at the spinneret. Because of confining inner solution evaporation and promoting whipping instability, the feed rate of sheath solution had a great impact on the size of the resulting fibers. Transitions took place if the sheath feed rate was too high, and branched fibers, beaded strings and large joint would appear in the resulting fibrous mats.

1.4.2 Hollow Fibers

Another application of co-axial electrospinning is to make hollow fibers. The concept of making hollow nanofibers is opposite to that illustrated in Figure 1.4. Here, the core is selectively removed instead of the sheath, to obtain hollow fibers (Figure 1.6).

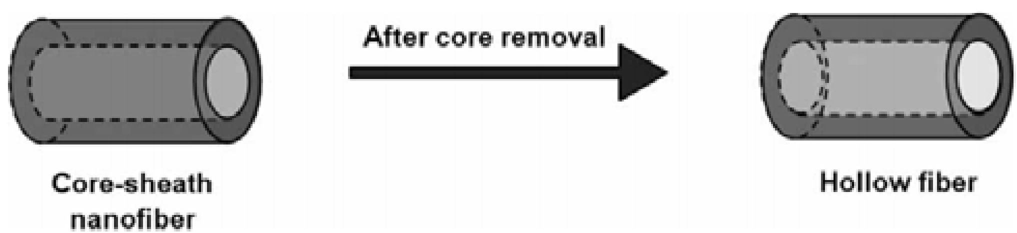

Figure 1.6 Schematic of formation of hollow fiber

The idea of producing hollow nanofibers using the co-axial electrospinning was first reported by Xia [20]. A combination of polyvinylpyrrolidone (PVP) and precursor $Ti(OiPr)_4$, dissolved in ethanol, which was used as the sheath solution. Heavy mineral oil was selected as the core solution. After hydrolysis of the precursor, simply by a prolonged exposure to air, the mineral oil was extracted by octane. The fiber was further calcinated to obtain pure titania hollow fibers (Figure 1.7). Based on Xia's papers, the core diameter and the sheath thickness were varied by changing the flow rate of the core. In a similar way, Loscertales [12] prepared the silica hollow fibers by using tetraethyl orthosilicate (TEOS) as the sheath. Kameoka [31] also reported the formation of nano-channels in silica nanofibers by co-axial electrospinning.

He used spin-on glass (SOG) and a PVP mixture in the sheath and motor oil in the core. After electrospinning, the core-sheath fiber was calcinated to remove PVP and motor oil and to form cross-linked SiO_2 hollow fibers.

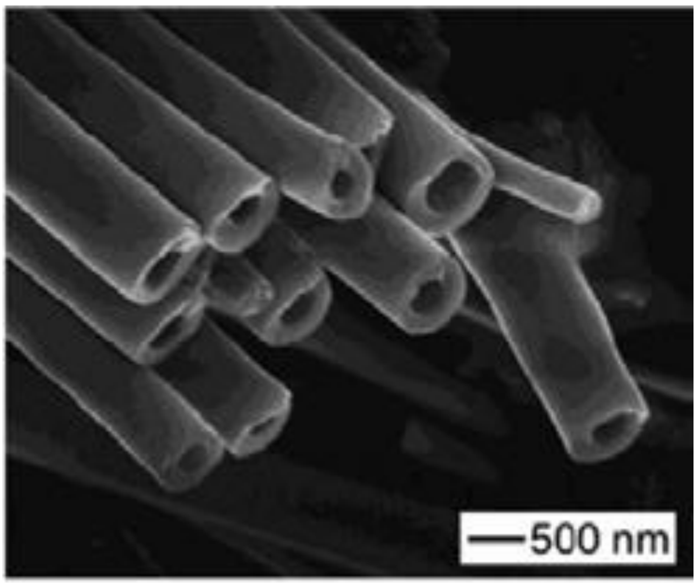

Figure 1.7 Hollow nanofibers prepared by co-axial electrospinning

1.4.3 Fibers Containing Particles

The major application of co-axial electrospinning may be in micro-encapsulation of the composites for biological application such as gene therapy, drug delivery and tissue engineering. Loading drugs through one-layer electrospun nanofibers are broadly reported since 2000. However, initial high releasing rate and later sharp decrease for drug releasing rate in one-layer electrospun fibers limit its practical use [30]. Therefore, the ideal structure for drug delivery purpose is that drug particles incorporating in a core and enwrapped by an additional barrier-sheath. Jiang [32] demonstrated a study using polycaprolactone (PCL) sheath and bovine serum albumin (BSA) or lysozyme doped poly(ethylene glycol) (PEG) core for drug delivery purpose. He concluded that the structure and the functionality of the released proteins were unaltered. In a more refined study, another paper from Jiang [33] reported that the release rate of the proteins encapsulated in the core could be tuned simply by altering the chemical composition of the sheath.

The particles are not limited to drug particles in biological applications but could also be metal/semiconductor particles utilizing in altering the physical or chemical properties of the resultant fibers. Song [34] used magnetic particles in nanofibers to obtain a nonwoven mat that had magnetic properties and could be used in a host of products, including smart materials. Xia [35] introduced a technique that combines the process of melt electrospinning with co-axial electrospinning in an effort to encapsulate the phase change materials (PCMs) into polymer sheath. Since PCMs can help control the temperature around its melting point during phase change, the core-sheath fibers with PCMs in core could be potential used in textiles in an effort to generate / release heat.

1.5 Polymer Crosslinking and Crosslinked Polymers in Co-axial Electrospinning

Polymers are large molecules that entangle with each other and exhibit properties different from other classes of materials. Polymer chains are typically linear, branched or crosslinked. In a crosslinked polymer, covalent bonds connect polymer chains with each other, and quite literally the molecular weight of such a polymer network approaches infinity. Polymers that have covalent crosslinks can either be soft (like a rubber band) or hard (like cured epoxy). One of the most common used crosslinked polymers in engineering applications is epoxy. Once fully crosslinked (Figure 1.9), epoxy form a network system in which all polymer chains interconnect with each other and cause the epoxy to become rigid and tough.

Figure 1.8 Crosslinking of epoxy

Co-axial electrospinning are commonly used to fabricate crosslinked polymers which is not electrospinnable alone. Lin [44] successfully fabricated ultrafine polydimethylsiloxane (PDMS) fibers after removing PVP sheath from PDMS-PVP core-sheath fibers. They put a hot plate under the collector during co-axial electrospinning, PDMS precursor hit the collector and cure immediately and formed crosslinked PDMS fibers. PDMS fibers showed superior elastic features and it might find applications for wounding healing, catalysis and bio-sensors. Similarly, Wang [45] prepared ultrafine epoxy fibers by removing PVP sheath from epoxy-PVP core-sheath fibers. She also brought up the idea that making functional epoxy fibers by doping functional agents such as carbon black and nanoparticles for diverse applications.

Crosslinked polymers combined with co-axial electrospinning are also widely applied in healing (or self-healing) coating product. In such core-sheath fibers, the core is usually incorporated with pre-crosslinked epoxy resin, and sheath could be any type of electrospinnable polymers. In cases where the failure mode is delamination, such type of core-sheath fiber will break and pre-crosslinked epoxy resins will flow out and inject the crack with uncured epoxy resin. Ideally, the uncured epoxy resin will cure, bonding the laminae and repairing the damage. Braun [42] successfully fabricated acrylated polyurethane resin in core and PVP in sheath core-sheath beaded fibers via co-axial electrospinning. Core-sheath beaded fibers were then added into polymer matrix to form final self-healing coating. Upon damage to the coating, core resins from the mechanically ruptured beads would release and flow into the scribed region. Passivation of substrate would complete once the core resin crosslinked at room temperature. Keller [43] also successfully fabricated epoxy-PVA core-sheath fibers via co-axial electrospinning. It is worth to state that Keller explained co-axial electrospinning process with Maxwell model and measured the fraction ratio of epoxy in core-sheath fiber by TGA both in experimental and theoretical way.

1.6 Introduction to Photothermal Effect of Gold Nanoparticles (AuNPs)

AuNPs attract much interest due to their unique properties, especially for large optical enhancements resulting in the strong scattering and absorption of light [38]. The enhancement in the optical properties of AuNPs arises from resonant oscillation of their free electrons in the presence of light, also known as surface plasmon resonance (SPR). The SPR are usually dependent on the size, shape, and degree of particle-to-particle coupling;

furthermore, the plasmon resonance can be rapidly converted to heat. The phenomenon of photothermal effect is the AuNPs are illuminated by light emitting in a specific wavelength, which makes the AuNPs generate a plasma resonance effect to convert light energy into thermal energy [39-41].

CHAPTER 2

Research Objective

The main objectives of the work are to:

(1) Fabricate bi-component core-sheath fibers with a pre-crosslinked epoxy/hardener in the core; and PMMA in sheath. The purpose of incorporation of an epoxy into electrospun fibers is to improve mechanical properties. In applications, the poor mechanical properties of electrospun fibers limit their potential use. Hence, applications such as filter in water purification system, or separator in Lithium-ion battery could be further developed.

(2) Determine the efficacy of Post-fabrication curing of the epoxy core. Two methodologies are investigated. First, a conventional curing method (oven heating) is evaluated. Here the outer surface of the electrospun fibers heated first, and then heat will transfer into the interior. Heat transfer is dependent on thermal conductivity of the sheath. Second, the photothermal effect on the pre-cured epoxy is investigated. Using the unique SPR properties of AuNPs, at a certain incident wavelength of light, AuNPs is able to cover light to thermal energy. At the same time, with the incorporation of AuNPs in core, heat will be generated from core and transfer from inside-out (we call this process photothermal curing). We expect that photothermal curing is more likely to fully crosslink the epoxy faster than conventional curing.

CHAPTER 3

Materials and Experimental Details

3.1 Materials

All materials used in this work are shown below (Table 3.1). All materials are used without further purification.

Table 3.1 Main polymers and solvents used in this work

Name	Mw	Density (g/ml)	Vendor
Poly(methyl methacrylate) (PMMA)	350,000	1.17	Sigma-Aldrich
Poly(ethylene oxide) (PEO)	400,000	1.21	Sigma-Aldrich
Polyacrylonitrile (PAN)	150,000	1.184	Sigma-Aldrich
Perylene	252.31	NA	Sigma-Aldrich
Dimethylformamide (DMF)	73.09	0.944	Sigma-Aldrich
Epoxy (D.E.R. 736)	NA	1.14	Dow
Hardener (D.E.H. 24)	NA	0.981	Dow

3.2 Experimental

3.2.1 Preparation of AuNPs

In this work, AuNPs solution is fabricated based on Frens' method [36]. Here, we want AuNPs dissolved in DMF instead of water, so a washing procedure is conducted prior to use:

1. Place AuNPs solution in 1.5ml centrifuge tube.

2. Centrifuge AuNPs for 30 minutes using the appropriate G force depending on size of the AuNPs (Table 3.2 [37]).

3. Remove clear water on top of centrifuge tube. Re-disperse AuNPs into DMF. To assure well dispersity, bath-sonication is performed subsequently.

Table 3.2 Appropriate G forces for centrifugation of AuNPs

Size (nm)	Speed (g)	Time (min)
5	100,000	30
10	17,000	60 (~50% recovery)
15	17,000	30
20	6,500	30
30	4,500	30
40	2,500	30
50	2,000	30
60	1,125	30
80	600	30

3.2.2 Preparation of Core and Sheath Solutions

PMMA is dissolved in DMF and magnetically stirred at $60^{o}C$ for 12 hours to obtain 10wt% PMMA solution which is used as sheath solution. The core solution is composed of epoxy, hardener, gold nanoparticles, and perylene. Freshly prepared water soluble AuNPs is centrifuged (Eppendord Centrifuge 54150) with a 4500 relative centrifugal force for 30 minutes. Approximate 1.4 ml water in the upper segment of the 1.5 ml centrifuge tube is removed, after which the concentrated AuNPs solution is dried up in a forced convection oven (LR Technologies LN6) at $60^{o}C$ for 2 hours to obtain completely dry gold nanoparticles. To prepare core solution, dry AuNPs is added into an epoxy and hardener solution (9:1 volume ratio of respective components), which has been partially cured at room temperature overnight. This epoxy-hardener-AuNPs solution is then mixed with DMF-dissolved perylene, and the resulting solution bath-sonicates for 15 minutes to ensure uniform dispersion of components. Here, the DMF serves not just as a vehicle for an introduction of perylene, but also to adjust (decrease) viscosity of partially cured epoxy-hardener solution. Perylene is used to monitor the temperature of the core materials (temperature estimated via observation of the fluorescence peak ratios during a photo-thermal annealing process, to be discussed in-depth later). In the final epoxy-hardener-AuNPs-perylene-DMF solution, the concentration of AuNPs, and perylene to epoxy-hardener are 0.022wt%, and 0.001wt%, respectively. The volume percentage of DMF to epoxy-hardener is 3:2.

3.2.3 Co-axial Electrospinning

Two vertically oriented syringe pumps (New Era Pump System, Inc.) are used to separately feed core and sheath materials for co-axial electrospinning (Figure 3.1). The core-sheath extrusion device is fabricated by concentrically orienting 20 and 16 gauge needles. The feed rate for sheath solution is fixed at 2.7 ml/h while the core solution feed rate is fixed at 0.3 ml/h. The concentric, core-sheath needle apparatus is connected to a 30 kV high voltage power supply (Gamma, Inc.). A grounded collector plate covered with a sheet of aluminum foil is placed 10 cm below the tip of the core-sheath needle apparatus. Typically, the voltage applied for electrospinning is between 9 and 11 kV. Following 2-3 hours of continuous electrospinning, fibrous mats are collected for further characterization. In addition to aluminum foil, fibers are also electrospun directly onto glass slides for bright-field and fluorescence optical microscopy. Fibrous mats electrospun onto the glass slides display the same morphology and dimensions as fibrous mats on aluminum foil.

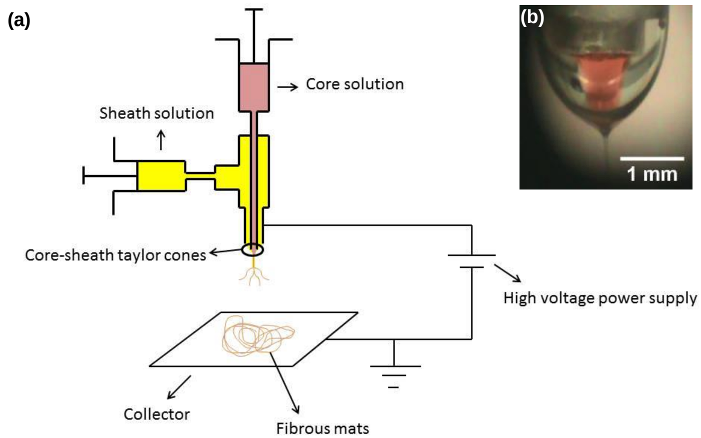

Figure 3.1 (a) Schematic illustration of the co-axial electrospinning set-up. (b) Core-sheath Taylor cones captured from recordings taken by Sony DCR-SR 681R camcorder. Reactive red 123 dye (Classic Dyestuffs, Inc.) was added into the core solution to simplify visual observation of Taylor cones

3.3 Characterization

3.3.1 Ultraviolet-visible Spectroscopy (UV-Vis)

Extinction spectra of AuNPs before and after centrifuging, core solution, and drop-cast films which are made up of core solution and conventional curing at 60^{o}C for 3 hours, are captured with an UV-Vis (CARY 50 Scan). These spectra are used to determine AuNPs plasmon and perylene absorption wavelengths.

3.3.2 Thermogravimetric Analysis (TGA)

To understand how long epoxy will be fully cured at 60^{o}C, TGA (Pyris 1, Perkin Elmer, Inc.) is conducted on epoxy films with 1, 2, 3, and 4 hours curing separately. Sample size is approximately 7.0 mg for each TGA experiment. The TGA instrument is ramped at 20^{o}C/min from 30 to 600^{o}C. All experiments are conducted at nitrogen atmosphere.

3.3.3 Scanning Electron Microscopy (SEM)

Nanofibers samples, collected on aluminum foil, are sputter coated by a K-550X sputter coater with Au/Pd having thickness of 100 Å to assist charge dissipation. Three types of SEM are used: JEOL 6400F Field Emission SEM (JEOL USA, Inc., Peabody, MA), PhenomTM (Phenom-World B.V. a, The Netherlands) and Verios XHR SEM (FEI, Inc. Hillsboro, OR). After coating, the samples are mounted on the SEM and focused, and viewed at magnification between 3000 - 40,000 times over their original sizes. Those images are the used to evaluate the fiber diameter and consistency.

ImageJ is used to measure the diameter of fibers. Firstly the scale is set based on the scaling bar on the SEM image, and then the line length function could figure out the fiber diameter. Averagely 60 fibers are measured in each SEM images.

The thickness of the fibrous mats is measured by a micrometer (Fowler 54-200-777), and its apparent density and porosity are calculated using the following equations:

Apparent density (g/cm^3) = $\frac{\text{Mass of fibrous mats (g)}}{\text{thickness (cm)}\times\text{area(cm}^2)}$

Porosity =$(1 - \frac{\text{apparent density (g/cm}^3)}{\text{bulk density (g/cm}^3)}) \times 100\%$

To observe core-sheath structure of bi-component electrospun fibers, the fiber mats are immersed in liquid nitrogen for instant freezing. While still in the liquid nitrogen bath, the specimens were poked at various places using sharp razor to fracture the fibers. This is done to induce differential fibrillation between the sheath and the core. The fractured specimens are then viewed under Verios SEM and FE-SEM as described earlier.

3.3.4 Transmission Electron Microscopy (TEM)

The diameters of AuNPs before and after centrifuging are measured using TEM (JEOL 2000 FX). To facilitate the TEM, AuNPs solution is applied to copper grids, and then dry up under a heat lamp for 10 minutes to evaporate water present prior to TEM use. Core-sheath fibers are directly spun onto TEM grids (copper grids coated with a layer of Formvar and carbon film (Ted Pella, PELCO 400 mesh grids)) during electrospinning process. TEM grids attached to the sample holder are inserted into TEM column for observation of core-sheath structure without other post-treatment.

3.3.5 "Temperature VS Time" Experiment of Epoxy during Curing Reaction

To detect exothermal energy generate by epoxy during curing reaction, 9:1 (volume ratio) epoxy-hardener solutions are mixed together and cured in an oven at 60^{o}C. A thermocouple submerges into the solution to monitor the temperature change as a function of curing time.

3.3.6 Fourier Transform Infrared Spectroscopy (FTIR)

FTIR (Nicolet 470, Thermo Electron Scientific Instruments LLC.) is performed in transmittance mode. The FTIR chamber is purged with dry air to eliminate water vapor. The data is collected in Attenuated Total Reflectance (ATR) mode using a Germanium/Diamond tip that directly contacted the sample, instead of using potassium bromide (KBr) powders mixed with the sample. The spectra are observed between 4000-700 cm^{-1}, with 64 scans having a resolution of 4 cm^{-1}. FTIR of pure PMMA powders, fully cured epoxy-hardener films, fully cured fibrous mats before and after washing are performed in order to characterize the composition.

3.3.7 Dynamic Mechanical Analysis (DMA)

DMA (Q800, TA Instruments, Inc.), in tension film mode, is used to measure the mechanical properties of the uncured, conventionally cured, and photo-thermally cured fibrous mats. The samples shape by cutting 6 mm width strips from the fibrous mats collected on the aluminum foil. All the measurements are carried out at a single frequency of 1 HZ with amplitude of 10 µm and clamp distance of 15 mm. The DMA capture data for a range of -60^{o}C to 250^{o}C with a heating rate of 3^{o}C/min.

3.3.8 Statistical Analyses

In this work, data comparison is characterized in a statistical way by using Softwares including SAS, Rstudio and StatCrunch.

CHAPTER 4

Results and Discussion

4.1 UV-Vis Result

The ultimate goal of this project is to separately cure epoxy core-sheath fibers with two methods – conventional curing and photothermal curing, and to compare the effect of the two types of curing on the morphology and mechanical properties of the resulting epoxy fibers. Herein, in order to eliminate the influence of AuNPs , we have AuNPs incorporated into the pre-crosslinked epoxy no matter what types of curing is followed by. TEM and UV-Vis is used to characterized the core solution.

TEM images show that the AuNPs before and after centrifuging are with a diameter of 19 $\pm$ 2.6 nm and 17 $\pm$ 1.6 nm, respectively. Figure 4.1 (a) shows that for AuNPs before and after centrifuging, the spectral location of the SPR are both at 532 nm.

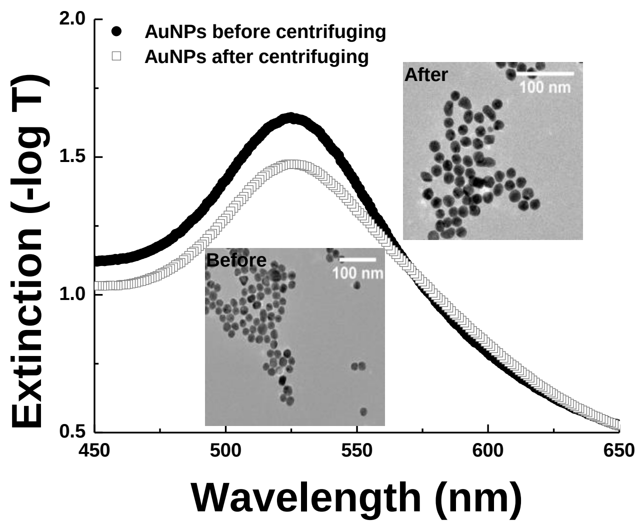

Figure 4.1 Extinction spectrum of the AuNPs in aqueous solution before and after centrifuging. TEM images of AuNPs before and after centrifuging, respectively

Normally, AuNPs tend to show bright pinkish color in water. However, after re-dissolving AuNPs into epoxy or DMF, the resulting solutions become slightly darker (Figure 4.2). We hypothesize the color changes resulting from two reasons: (1) after centrifuge, AuNPs aggregate at the bottom part of the centrifuge bottle. Removing water from the top part of the centrifuge tube and conducting a quick dry would not make AuNPs completely dry indeed. So, AuNPs still aggregate after re-dissoving into DMF or epoxy. Even though bath-sonication can disperse AuNPs better in DMF or epoxy, agglomeration cannot be totally avoided and the resulting solution will exhibit darker color. (2) Refractive index of water, DMF and epoxy are 1.33, 1.43 and 1.55, respectively. Hence, epoxy/AuNPs solution has a red shift than DMF/AuNPs (Figure 4.3). Based on our experience, 30 nm red shift of AuNPs from its original position (522nm) will not influence its SPR potency.

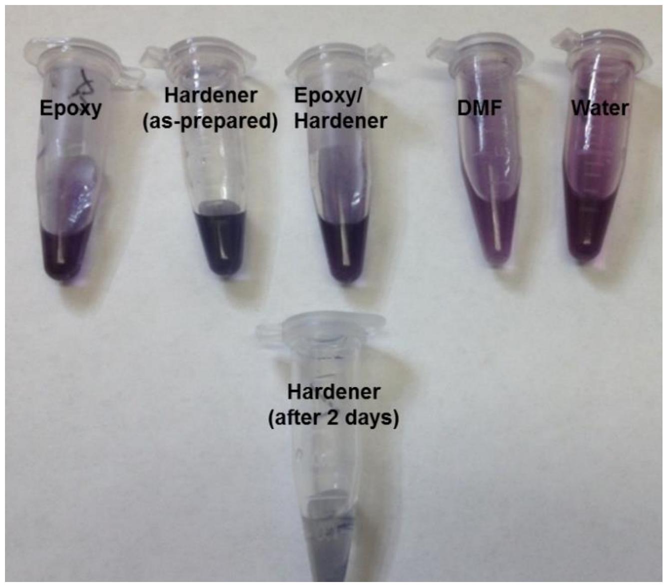

Figure 4.2 Top left to right: epoxy/AuNPs solution, hardener/AuNPs solution (as-prepared), epoxy-hardener/AuNPs solution, DMF/AuNPs solution, original AuNPs solution

Bottom: hardenr/AuNPs solution after 2 days

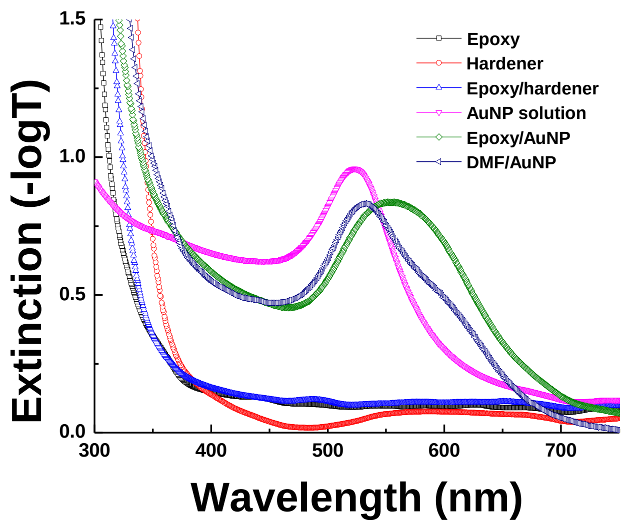

Figure 4.3 Extinction spectrum of epoxy, hardener, epoxy-hardener (9:1 volume ratio), original AuNPs solution, epoxy/AuNPs solution and DMF/AuNPs solution

However, in Figure 4.2, hardener/AuNPs solution is blueish as prepared and totally clear after 2 days. Figure 4.4 shows similar results. In as-prepared AuNPs/hardener solution, peak at 533 nm reflects AuNPs and peak at 676 nm reflects bluish complex formed in AuNPs/hardener solution. Gold is well known to be a stable element whereas AuNPs are not. Since AuNPs are in nano-scale, they have enough surface area to attach to hardener and form clathrate compounds. As the increase of time, gold peak becomes a shoulder, and the broad peak around 731 nm reflects the formation of the clathrate complex. Finally, we assume that reaction reaches equilibrium when the mixture solution becomes clear and UV-Vis curve does not change any more. In the final mixture solution, only a small amount of AuNPs remain and they no longer possess the ability of SPR.

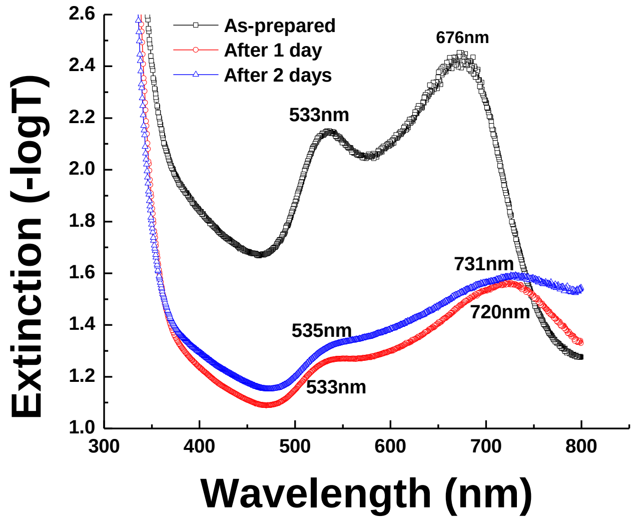

Figure 4.4 Extinction spectrum of the hardener/AuNPs solution as a function of time at room temperature

In order to avoid hardener attacking AuNPs, epoxy-hardener is pre-cured before mixing with AuNPs. In pre-cured epoxy-hardener solution, as majority of hardener has already been reacting with epoxy, AuNPs lose guest to form clathrate. A series of drop casting films are made and fully cured for UV-Vis. In Figure 4.5, as the increase of curing temperature, peak at 383 nm becomes more significant. That happens to all films no matter with or without AuNPs. Therefore, AuNPs play no role in the formation of peak at 383 nm. Temperature is the only factor here.

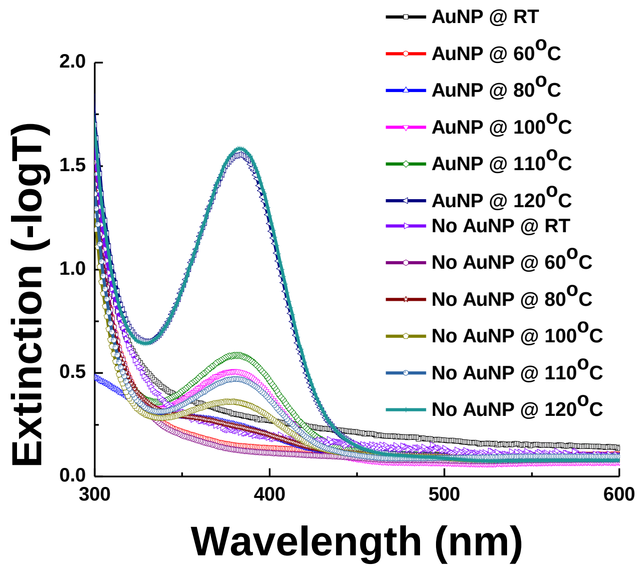

Figure 4.5 Extinction spectrum of epoxy-hardener (with/without AuNPs) drop-cast films at various temperature. Films are maintained at 3mm thick and fully cured before test

Here, we assume that the length (size) of cross-linked epoxy-hardener chains attributes to the formation of the peak at 383nm [47]. Mechanism of curing reaction is shown below.

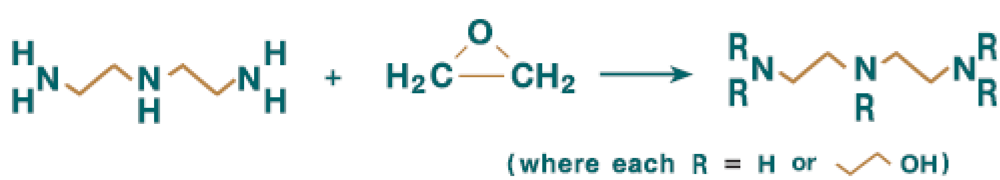

Increasing curing temperature will no doubt accelerate curing reaction. At high curing temperature, hardener acts like initiator in addition polymerization where long chains are formed and only a small amount of hardener are consumed to connect with epoxy groups. At low temperature, especially at room temperature, epoxy reacts with hardener in a moderate situation. Polymer chains tend to be short and majority of hardener will be consumed to form connections between epoxy and hardener during reaction. Therefore, we pre-cure epoxy-hardener solutions at room temperature before mixing with AuNPs in order to consume hardener and make AuNPs survival in mixing solutions. Figure 4.6 shows that with the help of pre-cure process, AuNPs survives in the epoxy-hardener solution. After drop casting films of the pre-cured core solution and have them fully cured at $60^{o}C$, AuNPs still show strong features.

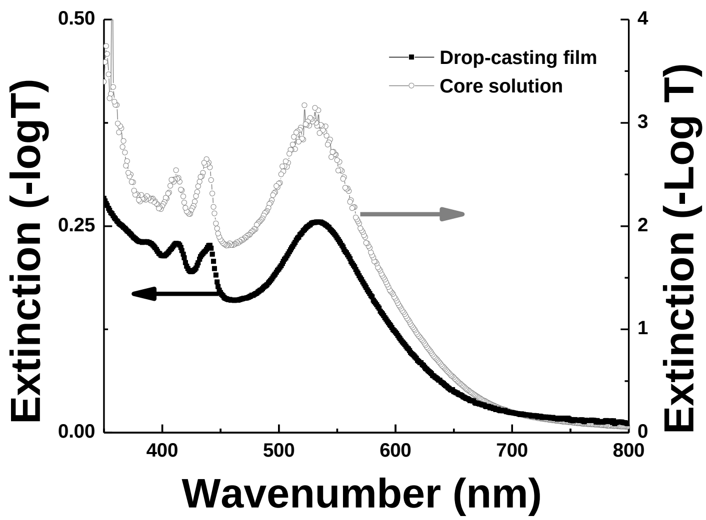

Figure 4.6 Extinction spectrum of the core solution and drop-casting film made up of core solution

4.2 TGA Result

TGA (Figure 4.7 and Table 4.1) is conducted to understand the effect of curing time on crosslink density of epoxy-hardener. Here, a series of epoxy-hardener drop-casting films are made from core solution and conventional cured at 60^{o}C for various curing time. 0h curing indicates as-prepared core solution. As discussed in the experimental section, 60v% of DMF is added into pre-cured epoxy-hardener solution in order to adjust its viscosity to a point which is sufficient low for co-axial electrospinning. Since boiling point of DMF is around 153^{o}C, the first sharp decrease of 0 hour curing sample in TGA reflects the evaporation of DMF. Once DMF completely evaporates at 153^{o}C, the curve goes into a plateau until the occurrence of decomposition. In 1 hour curing sample, the small fraction of decrease before

153^{o}C is due to the evaporation of DMF as well. The onset degradation temperatures for 5 samples are 304, 306, 312, 314 and 314^{o}C, respectively. Hence, it can be concluded that epoxy-hardener is fully cured at 60^{o}C for 2 hours. In core-sheath fibrous sample, since majority of DMF in core solution evaporates during co-axial electrospinning, core-sheath fibers are more likely of fully cured at 60^{o}C for less than 2 hours.

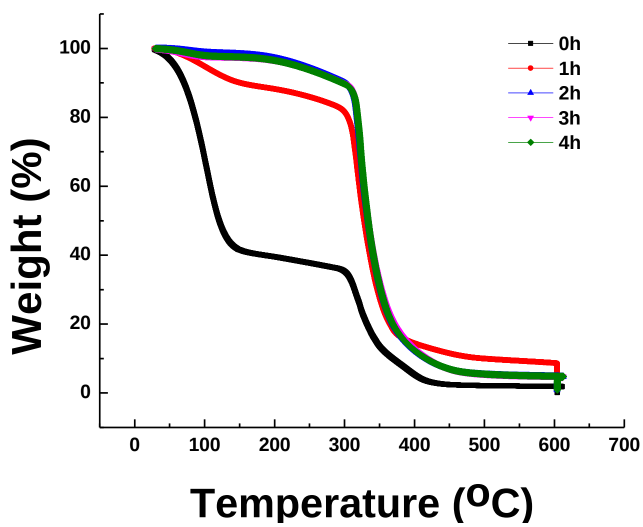

Figure 4.7 TGA graph of epoxy-hardener drop casting films obtained from core solution with various curing time at 60^{o}C

Table 4.1 Onset degradation temperature and weight of drop-casting epoxy films

Curing time (hour)	Onset degradation temperature (^oC)	Onset Weight (%)
0	304	36
1	307	82
2	313	89
3	314	89
4	315	89

Statistically, to determine that onset degradation temperature is not changing after 2 hours, if temperature (response) and time (predictor) should fit in a simple linear regression model that $y = \beta_0 + \beta_1 x + \varepsilon$ and β_1 equals 0, then it can be concluded that temperature is same for all time.

H_0: $\beta_1 = 0$. H_α: $\beta_1 \neq 0$. (H_0 is null hypothesis and H_α is alternative hypothesis)

P-value = $0.1616 > \alpha = 0.05$

Fail to reject H_0.

Therefore, $\beta_1 = 0$. Degradation temperature is not changing after 2 hours.

4.3 Effect of Curing Time on Epoxy-PMMA Core-sheath Fibers

After co-axial electrospinning, fibrous mats are cured at 60^oC in a conventional oven for various hours. As the increase of curing time, average fiber diameter does not change much (which can be seen in Table 4.2). However, it is clear that fiber morphology alters from smooth to unique as the increase of curing time. In Figure 4.10, fibers tend to agglomerate and twist with each other forming fiber bundles, unzipping (U-shape) and ribbon-like fibers after curing, whereas uncured fibers show relatively uniform (common) electrospun fiber morphology. We hypothesize the exothermal energy generated from epoxy during curing reaction attributes to the formation of these unique fiber structures [46]. Since PMMA has a glass transition temperature around 105^{o}C, exothermal energy is sufficient to "melt" PMMA, shrink and deform fibers, and lead to the formation of unique structures. In the meanwhile, as discussed in TGA results section, fibers are expected fully cured at 60^{o}C after 2 hours. Just from SEM images, it is hard to tell difference between fibers after 1 hour curing and fibers after 3 hour curing. This is mainly because majority of exothermal energy generated and released at the beginning of epoxy curing reaction, and this period tends to be short (less than 1 hour). Once exothermal energy is not sufficient to keep the temperature above the Tg of PMMA, fiber morphology will no more change.

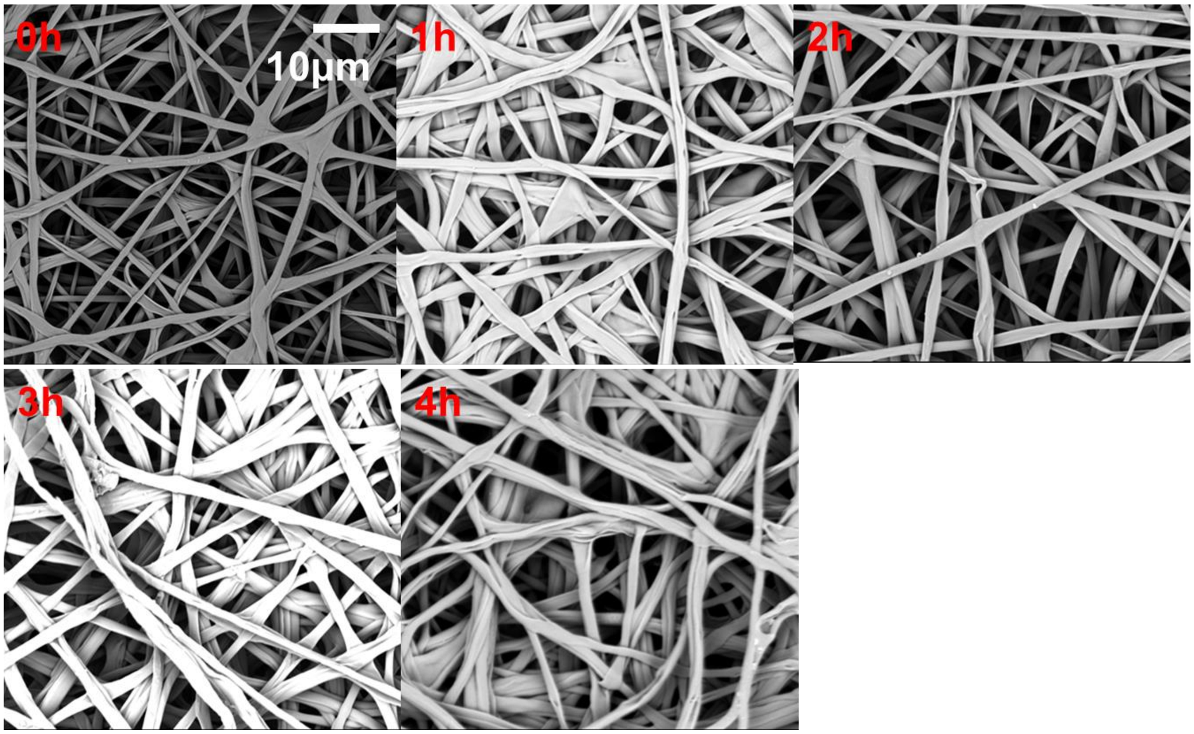

Figure 4.8 SEM images of epoxy-PMMA core-sheath fibers after conventional curing at 60^{o}C for 1, 2, 3, and 4 hours. 0h means uncured fibers

Similarly, to determine fiber diameter changes as a function of curing time, a simple linear regression model - $y = \beta_0 + \beta_1 x + \varepsilon$ is used.

H_0: $\beta_1 = 0$. H_α: $\beta_1 \neq 0$.

P-value=0.43 > 0.05.

Fail to reject H_0.

Therefore, it can be concluded that fiber diameter = 1.31 ± 0.30 µm. That being said, fiber diameter has no relationship with curing time.

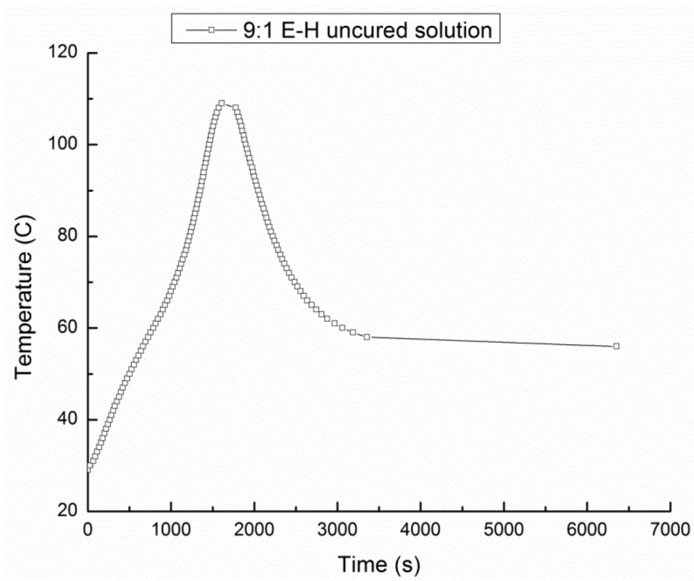

Figure 4.9 Temperature of epoxy solution at 60^{o}C as a function of time

Table 4.2 Average fiber diameter and porosity of pure PMMA fibers, epoxy-PMMA core-sheath fibers conventional cured for 0, 1, 2, 3 at 60^{o}C, and 4 hours, and washed fibers

Curing time (hour)	Fiber diameter (μm)	Porosity (%)
0	1.31 ± 0.33	78
1	1.32 ± 0.39	78
2	1.33 ± 0.22	79
3 (before washing)	1.32 ± 0.25	79
4	1.36 ± 0.29	80
Pure PMMA	0.61 ± 0.12	85
After washing	0.79 ± 0.21	0

In addition, the TEM image in Figure 4.11(a) shows the formation of core-sheath fibers with good contrast between epoxy and PMMA. It can be seen that the diameter of the entire fiber obtained is around 1.04 μm and the diameter of the core is around 0.35 μm. However, the contrast of U-shape fiber in Figure 4.11(b) reflects the thickness contrast under TEM.

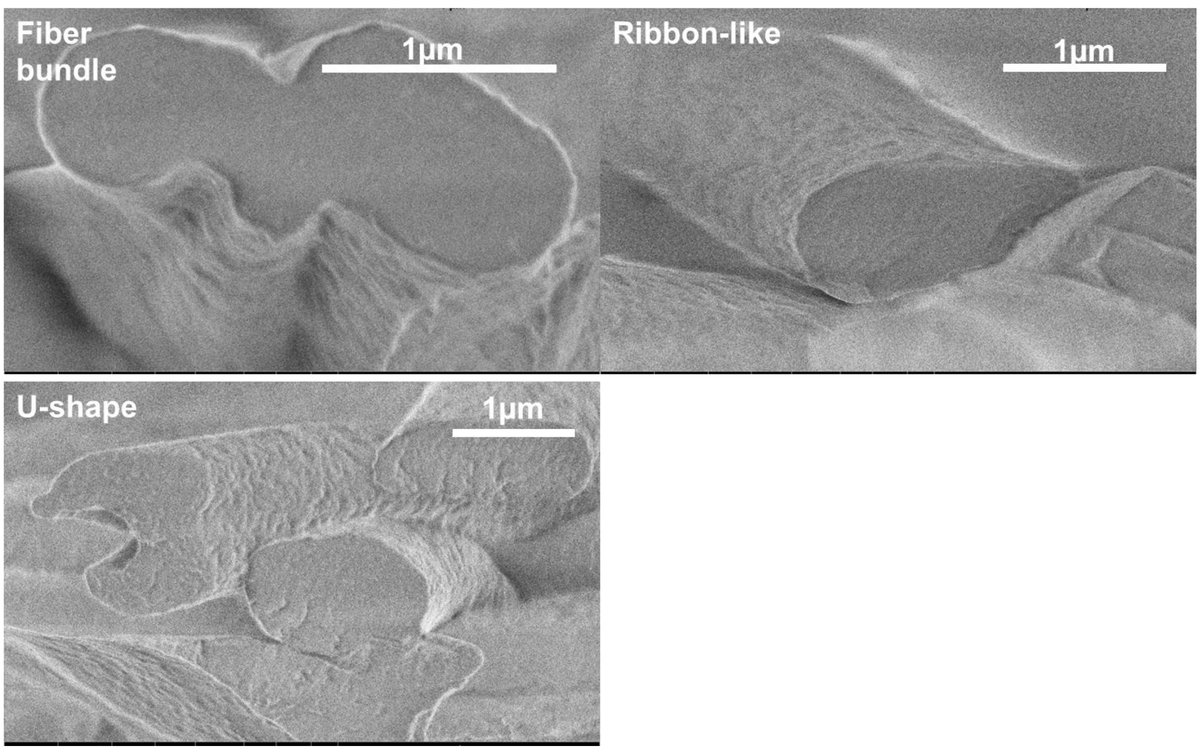

Figure 4.10 SEM images of cross-sections of fully cured epoxy-PMMA core-sheath fibers

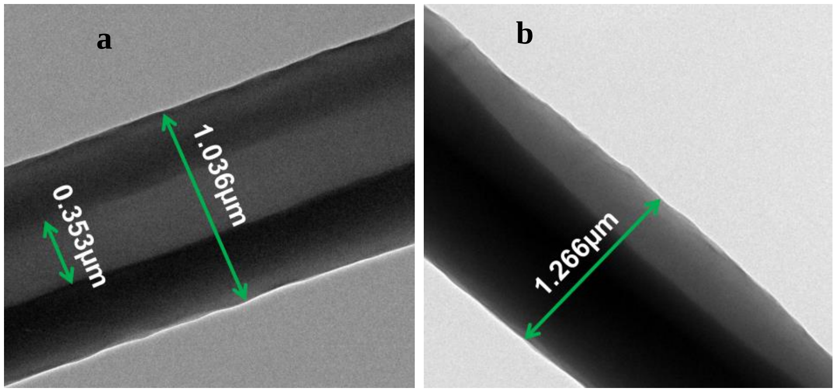

Figure 4.11 TEM images of (a) epoxy-PMMA core-sheath fibers, and (b) U-shape fibers

4.4 Removal of the Sheath

Fibers curing for 3 hours at 60^{o}C are believed fully cured and selected as fibers before washing. The washing process includes soaking fibers in DMF for 2 hour, and followed by rinsing with fresh DMF for 15 minutes, and followed by a quick dry in an oven at 60^{o}C for 10 minutes.

SEM images are taken to see fiber morphology after washing. Figure 4.12 shows that the structure and integrity of fibers are maintained after washing. Also, Table 4.2 shows that fiber diameter decreases from 1.32 μm to 0.79 μm after washing, which indicates that majority of PMMA sheath is removed after washing.

T-test is used to determine fiber diameter changes between fibers before and after washing.

H_0: Fiber diameter does not change after washing.

H_α: Not H_0.

P-value < 0.0001 < $\alpha = 0.05$

Reject H_0.

Therefore, it can be concluded that fiber diameter decrease after washing.

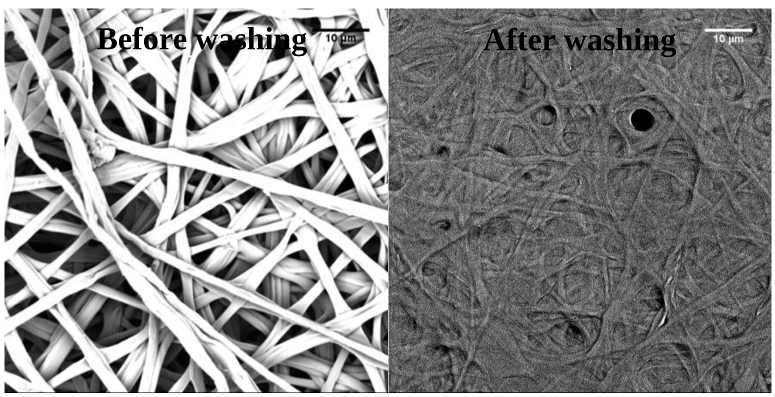

Figure 4.12 SEM images of fully cured epoxy-PMMA fibers before and after washing

4.5 FTIR Result

FTIR is conducted to determine the ingredients in fibers after washing. A drop casting epoxy-hardener film (from the core solution) is conventional cured at 60^oC for 3 hours, which is designated as the control. It is worth noting that peak at 3400 and 1650 cm^{-1} (violet line) reflect N-H group (stretch and bend, respectively) only existing in epoxy-hardener, and peak at 1730 cm^{-1} (black line) reflects C=O group which is corresponding to PMMA. In unwashed fibers, both epoxy-hardener and PMMA show their unique signals which indicate the presence of PMMA and epoxy-hardener. Interestingly, unwashed fiber sample is originally detected by a FTIR with Germanium tip and FTIR graph curve shows unobvious epoxy-hardener signal. This is because the fibers are in micro-scale. Germanium tip could only detect the surface of unwashed fibers. Diamond tip is then replaced which can undergo deeper and detect epoxy-hardener in the inner layer. Epoxy-hardener signals (peak at 3400 cm-1) are more pronounced after replacement of Diamond tip which can be seen in Figure 4.13(b). In washed fibers, N-H signals at 3400 and 1650 cm^{-1} are still obvious whereas C=O peak diminished which means majority of PMMA is removed after washing. The remaining PMMA may stay interstitial fiber space, or interior part of uneven core-sheath fiber which is hard to dissolve by washing.

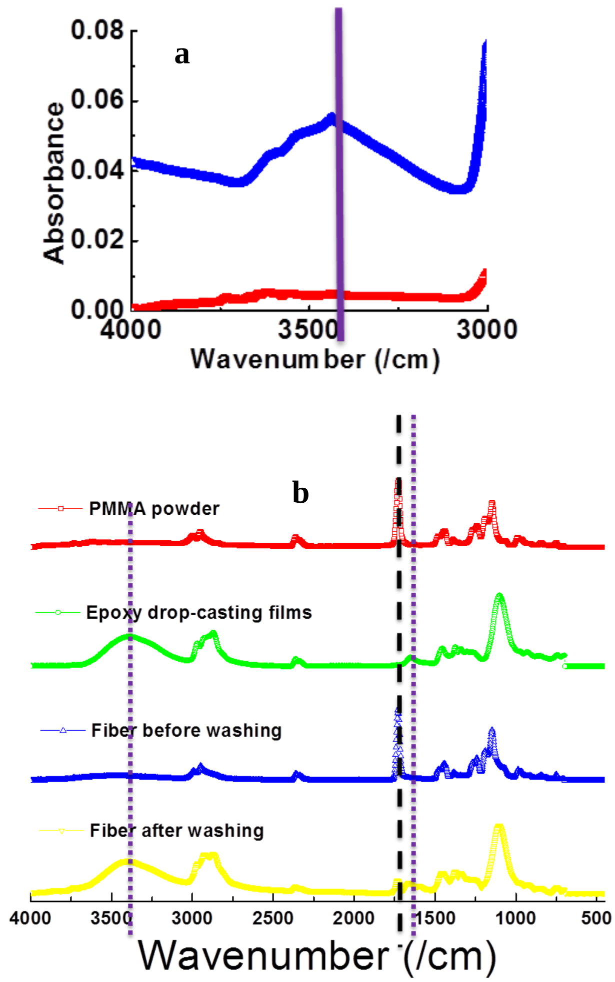

Figure 4.13 (a) Scale-up FTIR spectra of pure PMMA powder (red) and unwashed electrospun fibers (blue) with wavenumber falling in between 4000-3000 cm^{-1}. (b) FTIR spectra of pure PMMA powders, fully cured drop-casting epoxy-hardener films, fully cured PMMA/epoxy-hardener electrospun fibers before and after washing

4.5 DMA Result

Figure 4.14 (a) shows DMA results of pure PMMA electrospun fibers and epoxy-PMMA core-sheath fibers for various curing time at 60^{o}C. As the increase of curing time, the crosslinking density of epoxy core increase, and the epoxy core forms greater network structure. Hence, fibers after 3 hours curing yield the highest initial storage modulus and exhibits best mechanical property. It is clear that even uncured fibers (0h sample) exhibit better mechanical performance than pure PMMA electrospun fibers. This is mainly due to the incorporation of epoxy in to the PMMA.

Table 4.3 Storage modulus of fibers with different curing time, and fibers before and after washing, and pure PMMA fibers

Curing time (hour)	Storage modulus (MPa)
0	1342
1	2074
2	2718
3 (before washing)	3210
After washing	3868
Pure PMMA	88

Figure 4.14 DMA plots (a) storage modulus of fibers cured at 60^{o}C for 1, 2, 3 hours and pure PMMA fibers. (b) tan-delta of fibers cured at 60^{o}C for 1, 2, 3 hours and pure PMMA fibers (c) storage modulus of fibers before and after washing. For all DMA analysis, porosity of fibrous mats account for the modulus by equation $E_{measured} = E_{real} \times (1 - porosity)$

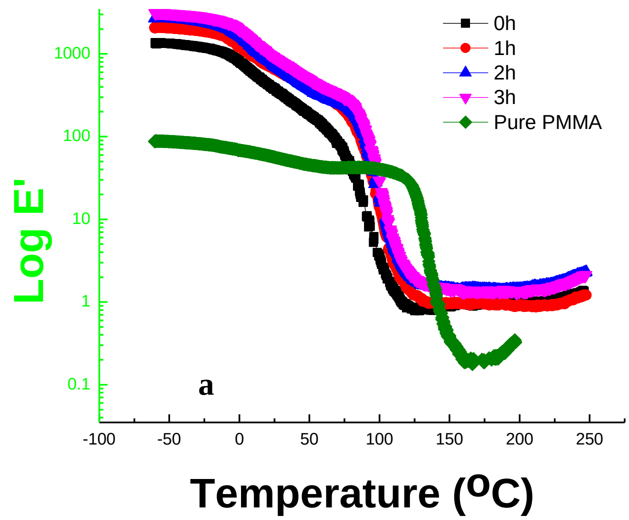
0h
1h
2h
3h
Pure PMMA
1000
100
10
1
0.1
Log E'
a
-100
-50
0
50
100
150
200
250
Temperature (^{O}C)

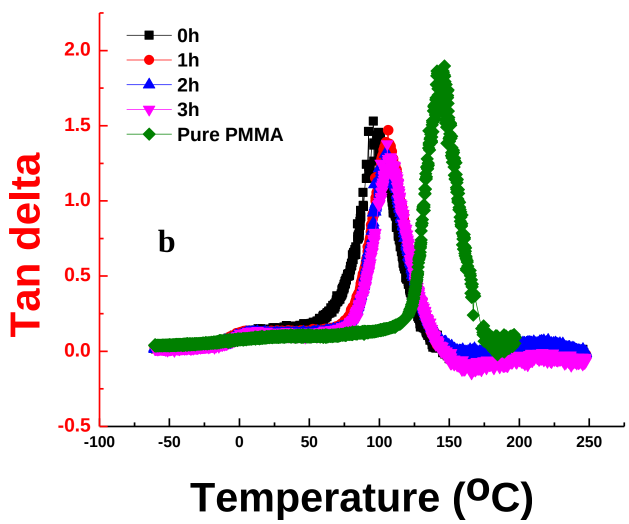
0h
1h
2h
3h
Pure PMMA
2.0
1.5
1.0
0.5
0.0
-0.5
Tan delta
b
-100
-50
0
50
100
150
200
250
Temperature (^{O}C)

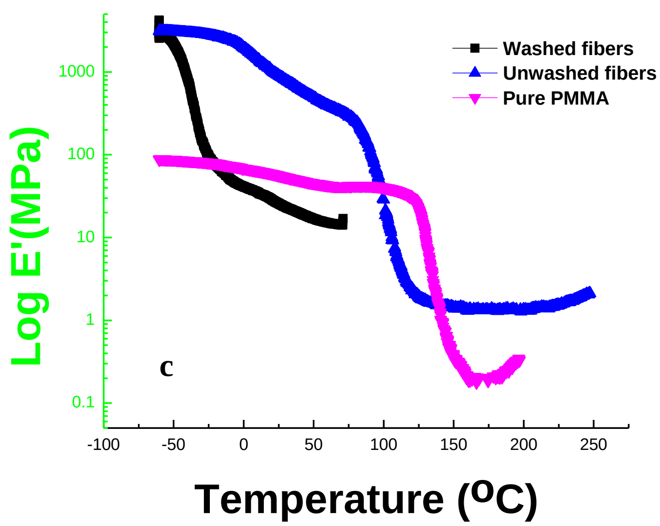

Log E'(MPa)
1000
100
10
1
0.1
-100
-50
0
50
100
150
200
250
Temperature (oC)
Washed fibers
Unwashed fibers
Pure PMMA
c

To determine porosity changes as a function of curing time, linear regression model is used.

H_0: $\beta_1 = 0$. H_α: $\beta_1 \neq 0$.

P-value = 0.0622 > 0.05

Fail to reject H_α.

Therefore, it can be concluded that porosity (%) = 77.86 ± 0.46. That being said, fibrous porosity does not change as a function of curing time.

According Figure 4.14 (b), the Tg of PMMA in core-sheath fibers is 105^{o}C, whereas the Tg of pure PMMA fibers is 145^{o}C. This is mainly because the plasticizer effect of remaining DMF in the core. Since the boiling temperature of DMF is around 153^{o}C, there will be more or less DMF left in the core after electrospinning and curing. That DMF goes into polymer networks and soft interaction among polymer chains. Therefore, Tg of PMMA has a left shift in core-sheath fibers.

Figure 4.14 (c) a comparison of core-sheath fibers before and after washing. Since majority of PMMA sheath is removed after washing, fibers after washing is mainly composed of epoxy, and fiber diameter is relatively thin (Table 4.2). Hence, fibers after washing break in the DMA furnace at 80^{o}C. According to Figure 4.14 (c) and Table 4.3, fibers before and washing have a comparable mechanical property, which is far more higher than that of pure PMMA fibers.

To analyze the relationship between modulus and curing time, simple linear regression and polynomial regression models are used.

Suppose y is modulus and x is curing time. $y = \beta_0 + \beta_1 x + \varepsilon$ (simple linear regression)

H_0: $\beta_1 = 0$. H_α: $\beta_1 \neq 0$.

P-value = 0.00372 < α = 0.05

Reject $H_{0.}$

Therefore, $\beta_1 \neq 0$. Modulus increase as the increase of curing time.

Suppose y is the modulus and x is the curing time. $y = \beta_0 + \beta_1 x + \beta_2 x^2 + \varepsilon$ (polynomial regression)

H_0: $\beta_2 = 0$. H_α: $\beta_2 \neq 0$.

P-value = 0.076 > α = 0.05

Reject $H_{0.}$

Therefore, $\beta_2 = 0$.

Hence, it can be concluded that the data do not fit in a quadratic model. That being said, modulus = 1399 + 624 × time. From 0 hour to 3 hour, modulus increases as a function of time. After 3 hours, since epoxy is fully cured, modulus is not changing.

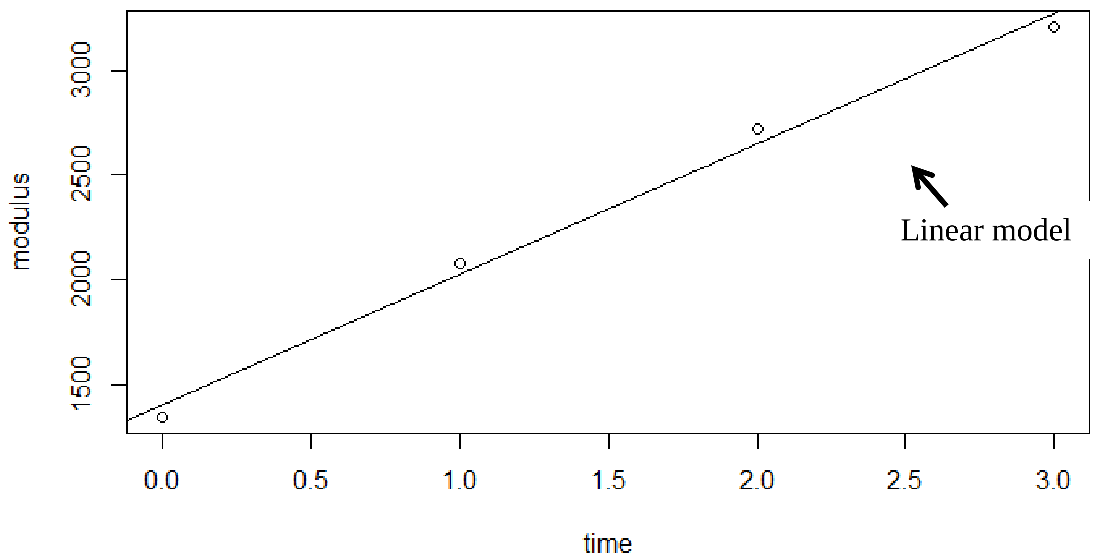

Figure 4.15 Relationship between curing time and modulus

CHAPTER 5

Conclusion

In summary:

(1) We successfully fabricated epoxy-PMMA core-sheath fibers via co-axial electrospinning. We determined that the miscibility, close viscosity between core and sheath solution, and high sheath-to-core flow rate ration contribute to the formation of core-sheath fibers.

(2) The core solution is made by mixing the AuNPs with partially cured epoxy-hardener solution (in order to avoid hardener attacking the AuNPs). With the help of SPR property of the AuNPs, heat will be generated from the core and transfer from inside-out at certain incident wavelength of light. Therefore, epoxy core will be cured in a photothermal way.

(3) Core-sheath morphology are confirmed via electron microscopy, and the decrease in fiber diameter after removing the PMMA sheath via washing, and the absence of PMMA peaks in the FTIR spectra after washing.

(4) For mechanical comparison, core-sheath fibers are stronger than pure PMMA fibers due to the incorporation of epoxy. Core-sheath fibers after 3 hours curing at 60^{o}C exhibit the best mechanical property due to the highest crosslink density of the epoxy core. Fully cured fibers before and after washing have a comparable mechanical property.

CHAPTER 6

Future Work

In the future, with the incorporation of AuNPs and perylene in the core, epoxy-PMMA core-sheath fibers will be photothermal cured. In the meanwhile, effect of photothermal curing parameters, such as laser intensity and curing time, on mechanical property of fibers will be studied systematically. Finally, the advantages of photothermal curing over conventional curing will be concluded.

REFERENCES

[1] Gilbert, W (1628) De Magnete, Magnetixisque Corporibus, et de Magno Magnete Tellure (On the Magnet and Magnetic Bodies, and on That Great Magnet the Earth), London, Peter Short.

[2] Cooley, F. Patent GB 06385 "Improved methods of and apparatus for electrically separating the relatively volatile liquid component from the component of relatively fixed substances of composite fluids" 19th May 1990.

[3] Taylor, G. (1964). Disintegration of water drops in an electric field. Proceedings of the Royal Society of London.Series A, Mathematical and Physical Sciences, 280(1382), 383-397.

[4] Taylor, G. (1966). The force exerted by an electric field on a long cylindrical conductor. Proceedings of the Royal Society of London.Series A, Mathematical and Physical Sciences, 291(1425), 145-158.

[5] Taylor, G. (1969). Electrically driven jets. Proceedings of the Royal Society of London.Series A, Mathematical and Physical Sciences, 313(1515), 453-475

[6] Li, D., & Xia, Y. (2004). Electrospinning of nanofibers: Reinventing the wheel? Advanced Materials, 16(14), 1151-1170.

[7] Morales, A. M., & Lieber, C. M. (1998). A laser ablation method for the synthesis of crystalline semiconductor nanowires. Science, 279(5348), 208-211.

[8] Jang, J., Lim, B., Lee, J., & Hyeon, T. (2001). Fabrication of a novel polypyrrole/poly(methyl methacrylate) coaxial nanocable using mesoporous silica as a nanoreactor. Chemical Communications, (01), 83-84.

[9] Xie, Y., Qiao, Z., Chen, M., Liu, X., & Qian, Y. (1999). Gamma-irradiation route to semiconductor/polymer nanocable fabrication. Advanced Materials, 11(18), 1512.

[10] (a) Bognitzki, M., Hou, H., Ishaque, M., Frese, T., Hellwig, M., Schwarte, C., Greiner, A. (2000). Polymer, metal, and hybrid nano- and mesotubes by coating degradable polymer template fibers (TUFT process). Advanced Materials, 12(9), 637.

(b) Hou, H., Jun, Z., Reuning, A., Schaper, A., Wendorff, J., & Greiner, A. (2002). Poly(p-xylylene) nanotubes by coating and removal of ultrathin polymer template fibers. Macromolecules, 35(7), 2429-2431.

(c) Liu, W., Graham, M., Evans, E., & Reneker, D. (2002). Poly(meta-phenylene isophthalamide) nanofibers: Coating and post processing. Journal of Materials Research, 17(12), 3206-3212.

[11] Caruso, R., Schattka, J., & Greiner, A. (2001). Titanium dioxide tubes from sol-gel coating of electrospun polymer fibers. Advanced Materials, 13(20), 1577.

[12] Diaz, J. E., Barrero, A., Marquez, M., & Loscertales, I. G. (2006). Controlled encapsulation of hydrophobic liquids in hydrophilic polymer nanofibers by co-electrospinning. Advanced Functional Materials, 16(16), 2110-2116.

[13] Yu, J., Fridrikh, S., & Rutledge, G. (2004). Production of submicrometer diameter fibers by two-fluid electrospinning. Advanced Materials, 16(17), 1562.

[14] Dror, Y., Salalha, W., Avrahami, R., Zussman, E., Yarin, A. L., Dersch, R., Wendorff, J. H. (2007). One-step production of polymeric microtubes by co-electrospinning. Small, 3(6), 1064-1073.

[15] (a) Chun, I., Reneker, D., Fong, H., Fang, X., Deitzel, J., Tan, N., & Kearns, K. (1999). Carbon nanofibers from polyacrylonitrile and mesophase pitch. Journal of Advanced Materials, 31(1), 36-41.

(b) Doshi, J., & Reneker, D. (1995). Electrospinning process and applications of electrospun fibers. Journal of Electrostatics, 35(2-3), 151-160.

(c) Fang, X., & Reneker, D. (1997). DNA fibers by electrospinning. Journal of Macromolecular Science-Physics, B36(2), 169-173.

(d) Hou, H., & Reneker, D. (2004). Carbon nanotubes on carbon nanofibers: A novel structure based on electrospun polymer nanofibers. Advanced Materials, 16(1), 69.

(e) Kim, J., & Reneker, D. (1999). Mechanical properties of composites using ultrafine electrospun fibers. Polymer Composites, 20(1), 124-131.

(f) Koombhongse, S., Liu, W., & Reneker, D. (2001). Flat polymer ribbons and other shapes by electrospinning. Journal of Polymer Science Part B-Polymer Physics, 39(21), 2598-2606.

(g) Yarin, A., Koombhongse, S., & Reneker, D. (2001). Taylor cone and jetting from liquid droplets in electrospinning of nanofibers. Journal of Applied Physics, 90(9), 4836-4846.

(h) Yarin, A., Koombhongse, S., & Reneker, D. (2001). Bending instability in electrospinning of nanofibers. Journal of Applied Physics, 89(5), 3018-3026.

(i) Reneker, D., & Chun, I. (1996). Nanometre diameter fibres of polymer, produced by electrospinning. Nanotechnology, 7(3), 216-223.

(j) Reneker, D., Yarin, A., Fong, H., & Koombhongse, S. (2000). Bending instability of electrically charged liquid jets of polymer solutions in electrospinning. Journal of Applied Physics, 87(9), 4531-4547.

[16] Townsend-Nicholson, A., & Jayasinghe, S. N. (2006). Cell electrospinning: A unique biotechnique for encapsulating living organisms for generating active biological microthreads/scaffolds. Biomacromolecules, 7(12), 3364-3369.

[17] He, C., Huang, Z., Han, X., Liu, L., Zhang, H., & Chen, L. (2006). Coaxial electrospun poly(L-lactic acid) ultrafine fibers for sustained drug delivery. Journal of Macromolecular Science, Part B: Physics, 45(4), 515-524.

[18] Zhang, Y., Huang, Z., Xu, X., Lim, C, & Ramakrishna, S. (2004). Preparation of Core−Shell Structured PCL-r-Gelatin Bi-Component Nanofibers by Coaxial Electrospinning. Chemistry of Materials, 16(18), 3406-3409.

[19] Sun, Z., Zussman, E., Yarin, A., Wendorff, J., & Greiner, A. (2003). Compound core-shell polymer nanofibers by co-electrospinning. Advanced Materials, 15(22), 1929.

[20] Li, D., & Xia, Y. (2004). Direct fabrication of composite and ceramic hollow nanofibers by electrospinning. Nano Letters, 4(5), 933-938.

[21] Huang, Z., Zhang, Y., & Ramakrishna, S. (2005). Double-layered composite nanofibers and their mechanical performance. Journal of Polymer Science Part B-Polymer Physics, 43(20), 2852-2861.

[22] Li, D., McCann, J., & Xia, Y. (2005). Use of electrospinning to directly fabricate hollow nanofibers with functionalized inner and outer surfaces. Small, 1(1), 83-86.

[23] Fong, H., Chun, I., & Reneker, D. (1999). Beaded nanofibers formed during electrospinning. Polymer, 40(16), 4585-4592.

[24] Hohman, M. M., Shin, M., Rutledge, G., & Brenner, M. P. (2001). Electrospinning and electrically forced jets. II. applications. Physics of Fluids, 13(8), 2221-2236.

[25] Moghe AK, Gluck JM, Gupta BS, King MW (2005) Electrospun Bicomponent Fibers for Soft Tissue Engineering: Book of Abstracts, The Fiber Society Fall 2005 Annual Meeting and Technical Conference, Newark NJ, USA 73-74.

[26] Wang, M., Yu, J., Kaplan, D., & Rutledge, G. (2006). Production of submicron diameter silk fibers under benign processing conditions by two-fluid electrospinning. Macromolecules, 39(3), 1102-1107.

[27] Ojha, S. S., Stevens, D. R., Hoffman, T. J., Stano, K., Klossner, R., Scott, M. C., Gorga, R. E. (2008). Fabrication and characterization of electrospun chitosan nanofibers formed via templating with polyethylene oxide. Biomacromolecules, 9(9), 2523-2529.

[28] Ojha, S. S., Stevens, D. R., Stano, K., Hoffman, T., Clarke, L. I., & Gorga, R. E. (2008). Characterization of electrical and mechanical properties for coaxial nanofibers with poly(ethylene oxide) (PEO) core and multiwalled carbon nanotube/PEO sheath. Macromolecules, 41(7), 2509-2513.

[29] Yu, D., Branford-White, C. J., Chatterton, N. P., White, K., Zhu, L., Shen, X., & Nie, W. (2010). Electrospinning of concentrated polymer solutions. Macromolecules, 43(24), 10743-10746.

[30] Loscertales, I., Barrero, A., Marquez, M., Spretz, R., Velarde-Ortiz, R., & Larsen, G. (2004). Electrically forced coaxial nanojets for one-step hollow nanofiber design. Journal of the American Chemical Society, 126(17), 5376-5377.

[31] Wang, M., Jing, N., Su, C., Kameoka, J., Chou, C., Hung, M., & Chang, K. (2006). Electrospinning of silica nanochannels for single molecule detection. Applied Physics Letters, 88(3), 033106.

[32] Jiang, H., Hu, Y., Li, Y., Zhao, P., Zhu, K., & Chen, W. (2005). A facile technique to prepare biodegradable coaxial electrospun nanofibers for controlled release of bioactive agents. Journal of Controlled Release, 108(2-3), 237-243.

[33] Jiang, H., Hu, Y., Zhao, P., Li, Y., & Zhu, K. (2006). Modulation of protein release from biodegradable core-shell structured fibers prepared by coaxial electrospinning. Journal of Biomedical Materials Research Part B-Applied Biomaterials, 79B(1), 50-57.

[34] Song, T., Zhang, Y. Z., & Zhou, T. J. (2006). Fabrication of magnetic composite nanofibers of poly(epsilon-caprolactone) with FePt nanoparticles by coaxial electrospinning. Journal of Magnetism and Magnetic Materials, 303(2), E286-E289.

[35] McCann, J. T., Marquez, M., & Xia, Y. (2006). Melt coaxial electrospinning: A versatile method for the encapsulation of solid materials and fabrication of phase change nanofibers. Nano Letters, 6(12), 2868-2872.

[36] Frens, G. (1973). Controlled Nucleation for the Regulation of the Particle Size in Monodisperse Gold Suspensions. Nature Physical Science, 241, 20-22.

[37] http://cytodiagnostics.com/store/pc/Gold-Nanoparticle-Handling-and-Storage-d7.htm

[38] Cheng, Y., Uang, R., Wang, Y., Chiou, K., & Lee, T. (2009). Laser annealing of gold nanoparticles thin film using photothermal effect. Microelectronic Engineering, 86(4-6), 865-867.

[39] Govorov, A. O., Zhang, W., Skeini, T., Richardson, H., Lee, J., & Kotov, N. A. (2006). Gold nanoparticle ensembles as heaters and actuators: Melting and collective plasmon resonances. Nanoscale Research Letters, 1(1), 84-90.

[40] Jain, P. K., El-Sayed, I. H., & El-Sayed, M. A. (2007). Au nanoparticles target cancer. Nano Today, 2(1), 18-29.

[41] Govorov, A. O., & Richardson, H. H. (2007). Generating heat with metal nanoparticles. Nano Today, 2(1), 30-38.

[42] Park, J., & Braun, P. V. (2010). Coaxial electrospinning of self-healing coatings. Advanced Materials, 22(4), 496.

[43] Mitchell, T. J., & Keller, M. W. (2013). Coaxial electrospun encapsulation of epoxy for use in self-healing materials. Polymer International, 62(6), 860-866.

[44] Niu, H., Wang, H., Zhou, H., & Lin, T. (2014). Ultrafine PDMS fibers: Preparation from in situ curing-electrospinning and mechanical characterization. Rsc Advances, 4(23), 11782-11787.

[45] Wang, X., Zhang, W., Yu, D., Li, X., & Yang, H. (2013). Epoxy resin nanofibers prepared using electrospun Core/Sheath nanofibers as templates. Macromolecular Materials and Engineering, 298(6), 664-669.

[46] Zhang, X., Yi, X., & Xu, Y. (2008). Cure-induced phase separation of epoxy/DDS/PEK-C composites and its temperature dependency. Journal of Applied Polymer Science, 109(4), 2195-2206.

[47] Anders, U., Nuyken, O., & Buchmeiser, M. (2003). Influence of chain length and temperature on UV-vis absorption and degradation behavior of poly(diethyl dipropargylmalonate) with an alternating cis-trans-1,2-(cyclopent-1-enylene)vinylene structure. Designed Monomers and Polymers, 6(2), 135-143.

APPENDIX

Appendix A. Histograms of Fiber Diameter Distribution

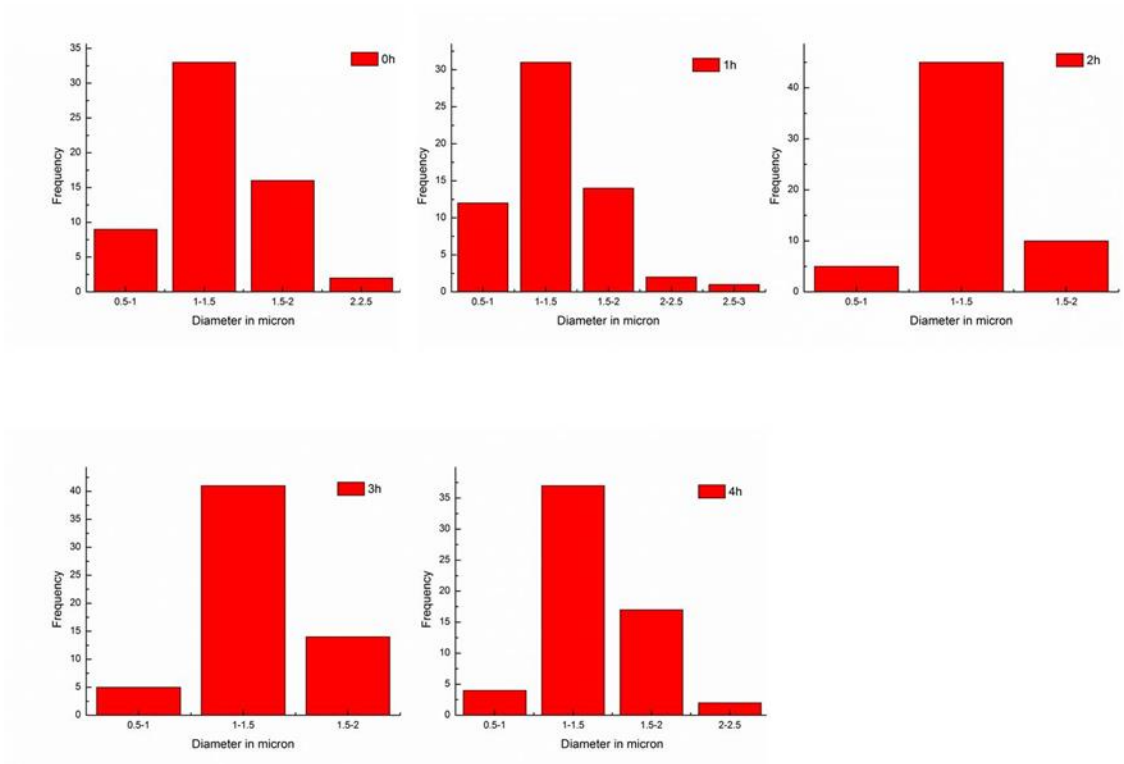

Figure A1 Histograms of fiber diameter distribution of epoxy-PMMA core-sheath fibers after conventional curing at 60^{o}C for 1, 2, 3, and 4 hours

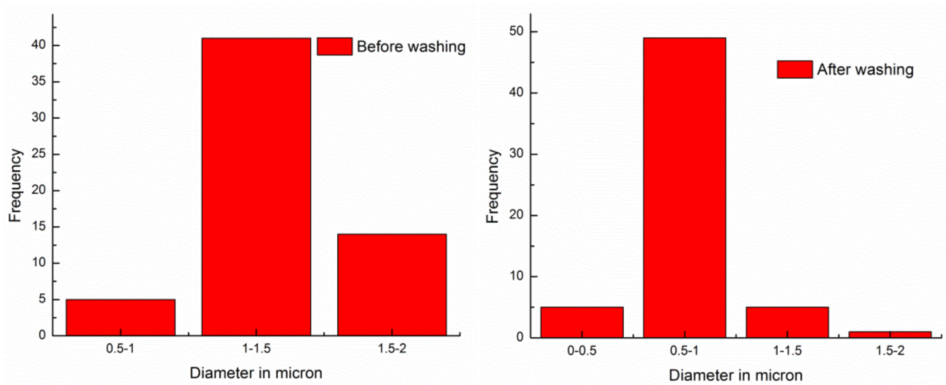

Figure A2 Histograms of fiber diameter distribution of epoxy-PMMA core-sheath fibers before and after washing

Appendix B. PEO-PAN Core-sheath Nanofibers via Co-axial Electrospinning

We tried to fabricate PEO-PAN core-sheath nanofibers via co-axial electrospinning before epoxy-PMMA core-sheath fibers. Since both PEO and PMMA are electrospinnable by themselves and they are both compatible with DMF, we believe that will help us better understand co-axial electrospinning process.

Figure B1 showed five different Taylor cone patterns as function of applied voltage during co-axial electrospinning. Figure B1 (c) showed two Taylor cones and one jet, which we defined as stable Taylor cones. Shape of stable Taylor cones would never change and the jet would continuous emit from tip of the tip of the needle. Figure B1 (b) and (d) showed two types of unstable Taylor cones respective at low and high applied voltage. At low voltage, the Taylor cones moved back and forth, and jet discontinuous came out from the tip of needle, and formed fibers on the collector after enlongation and whipping section. However, since the Taylor cones were not stable, the core and sheath solutions tended to mixed and therefore, forming uneven and ununiformed core. Under optimal and standardized co-axial electrospinning condition, electrical force and surface tension applied to the sheath solution were at equilibrium. As increasingly free charges in the core cone transferring to the sheath cone, the sheath cone moved forward once electrical force became stronger than surface tension. The core cone then moved forward due to the pushing force coming from syringe pump. As the sheath being drawn, contacting areas of two cones increased which would induce the increase of interfacial viscous force. As long as the sheath was strong enough to hold the core, the droplet would keep moving forward until it either falls down caused by the gravity, or ejected jet. Hence, we defined lower critical voltage as which was just strong enough to form two Taylor cones.

On the other hand, Figure B1 (d) showed unstable Taylor cones at high voltage. In such condition, electrical force was so strong that sheath Taylor cone did not have a chance to extend, but formed jet and emitted at the tip of core nozzle. In Figure B1 (e), increasing voltage would further cause the failure of the formation of Taylor cone. The sheath solution flowed into inner nozzle, mixing with the core solution and emitted a blend jet.

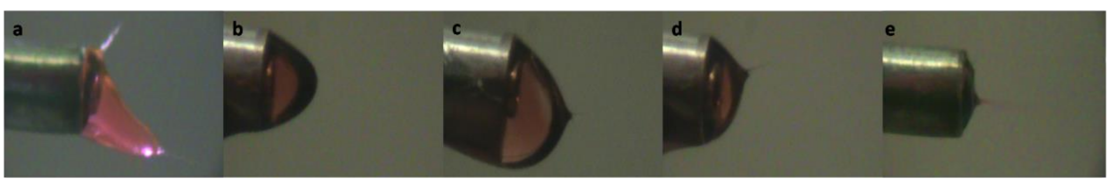

Figure B1 Shape of Taylor cones at various applied voltage (a. Taylor cones below lower critical voltage; b. Unstable Taylor cones above lower critical voltage; c. Stable Taylor cones; d. Unstable Taylor cones below upper critical voltage; e. Taylor cones above upper critical voltage)

To understand the relationship between stability of Taylor cone and formation of core-sheath structure, the PEO core got removed by heating core-sheath nanofibers in furnace under the protection of argon. Figure B2 (a) showed FESEM image of fibers emitted from stable

Taylor cones after heating. Here, the hollow core possessed a diameter of 100 nm and the wall thickness was 110 nm. Likewise, shallow pores with average diameter 100 nm can also be seen both inside and on the surface of fibers in Figure B2 (c). Since PEO component random distributed in the fibers, after heating, PEO completely disappeared, and the pores formed at the place where were originally occupied by PEO. TEM image (Figure B2 (d)) also showed that bubbles existed both on the surface and inside of the nanofibers, which also proved the statement.

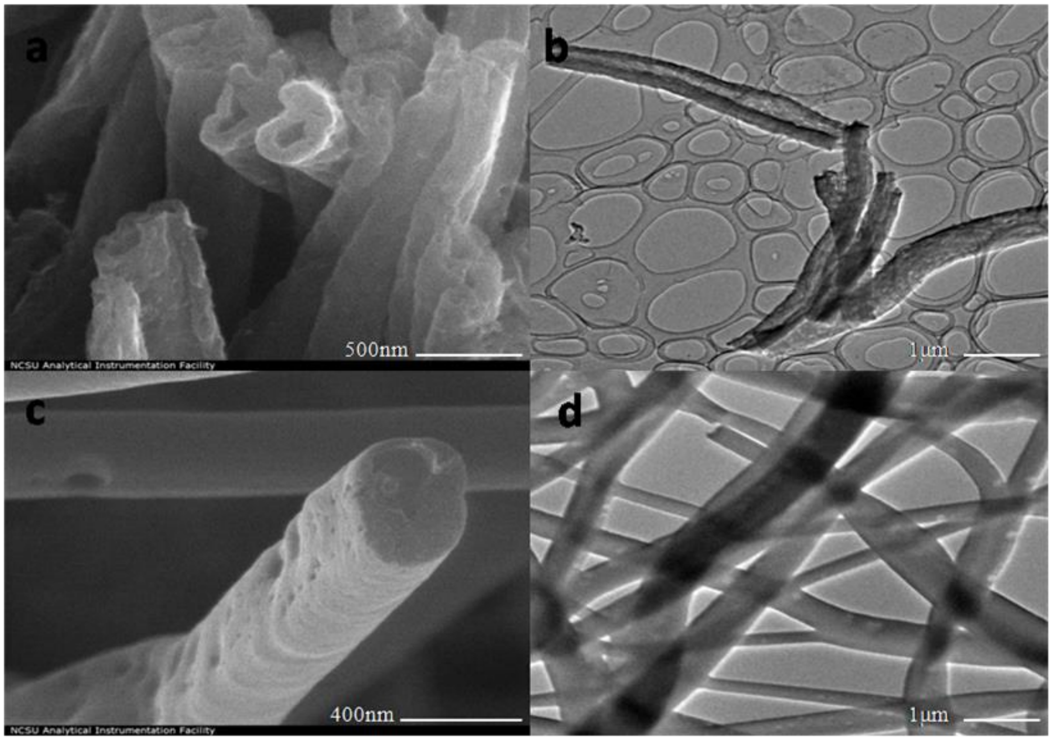

Figure B2 Microscopy images of core-sheath nanofibers after heating and carbonization (a. FESEM image of carbon nanotubes derived by heating and carbonizing PEO-PAN core-sheath nanofibers emitted from stable Taylor cones; b.TEM image of carbon nanotubes in corresponding with a; c. FESEM image of nanofibers after heating. The original core-sheath nanofibers were emitted from stable Taylor cones; d.TEM image of the nanofibers in c)

Figure B2 (b) showed that hollow core performed relatively even, uniform and continuous along the sheath. Hence, hollow fibers were well designed and fabricated with the help of heating of PEO-PAN core-sheath nanofibers emitted from stable Taylor cones.